Results in Engineering 26 (2025) 104753

Contents lists available at ScienceDirect

Results in Engineering

journal homepage: www.sciencedirect.com/journal/results-in-engineering

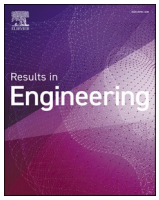

Research paper

Viscoelastic and structural insights into magnetorheological foam fabricated with different volumes of constraint foaming process

Ainaa Amirah Marzuki [a], Nur Azmah Nordin [a,b,*], Saiful Amri Mazlan [a,b], Mohd Aidy Faizal Johari [a], Michal Sedlacik [c,d,**], Siti Aishah Abdul Aziz [e], Abdul Yasser Abd Fatah [f], Shahir Mohd Yusuf [a]

[a] Engineering Materials and Structures (eMast) iKhoza, Malaysia – Japan International Institute of Technology (MJIIT), Universiti Teknologi Malaysia, Jalan Sultan Yahya Petra, 54100 Kuala Lumpur, Malaysia
[b] Automotive Development Centre, Institute for Sustainable Transport (IST), Universiti Teknologi Malaysia, 81310 Skudai, Johor, Malaysia
[c] Centre of Polymer Systems, University Institute, Tomas Bata University in Zlín, Trida T. Bati 5678, 760 01, Zlín, Czech Republic
[d] Department of Production Engineering, Faculty of Technology, Tomas Bata University in Zlín, Vavreckova 275, 760 01, Zlín, Czech Republic
[e] Faculty of Applied Sciences, Universiti Teknologi MARA (UiTM) Cawangan Pahang, Kampus Jengka, 26400 Bandar Tun Abdul Razak, Jengka, Pahang, Malaysia
[f] Department of Smart Engineering and Advanced Technology, Faculty of Artificial Intelligence, Universiti Teknologi Malaysia, Jalan Sultan Yahya Petra, 54100 Kuala Lumpur, Malaysia

ARTICLE INFO

Keywords:
Magnetorheological foam
Constraint volume foaming process
Storage modulus
Damping
Dynamic mechanical compression
Rheology
Morphology

ABSTRACT

Magnetorheological (MR) foam, a smart magnetic-responsive flexible polyurethane material, has garnered significant attention for its potential in soft robotics. However, limited studies on its dynamic mechanical and damping properties hinder its development for broader applications. This study investigates the influence of constraint volume foaming process (100 %, 75 %, and 50 % volume) on the properties of MR foam containing 75 wt. % carbonyl iron particles (CIPs) under dynamic mechanical compression and rheological shear testing at frequencies ranging from 0.1 to 10 Hz. Results showed that the constrained foaming MR foam with 50 % volume exhibited the most significant enhancement in storage modulus (E' and G'), attributed to a more compact CIP distribution, resulting in the lowest initial loss factor (tan δ). However, upon increasing frequencies, a notable increase of approximately 20 % in tan δ was observed for this MR foam, indicating improved energy dissipation at higher frequencies. In contrast, the free foaming MR foam demonstrated only a 5 % increase in tanδ, highlighting its lower energy dissipation capability. Morphological analysis revealed that constraint volume foaming process produced smaller pores and denser CIP distributions. The compact structure enhanced particle-matrix interactions, increasing friction and contributing to improved damping at elevated frequencies. In summary, the incorporation of constraint volume foaming process significantly enhanced the dynamic mechanical, rheological, and structural properties of MR foam. These advancements broaden its applicability for advanced applications, particularly in soft robotics, where energy dissipation and tunable properties are critical.

1. Introduction

In this notable world of advanced technology, the demand for smart soft robotics applications has significantly increased the consumer preference for devices such as soft robotic grippers. Soft robotics introduces a new category of robots capable of addressing challenges that traditional rigid robots cannot overcome. A high adaptability to operate in a complex environment and handling of delicate objects without causing a damage are some of the advantages they offer [1]. Owing to their high flexibility, lightweight, and versatile characteristics, porous materials such as composite foam has emerged as an innovative and efficient solution. These porous materials combine the benefits of the foam and composites, meeting the material's requirement as soft robotic grippers [2]. Generally, composite foams are comprised of reinforcing particles that are incorporated into a foam as a matrix material [3]. Foams have the ability to provide excellent structural integrity,

* Corresponding author at: Engineering Materials and Structures (eMast) iKhoza, Malaysia – Japan International Institute of Technology (MJIIT), Universiti Teknologi Malaysia, Jalan Sultan Yahya Petra, 54100 Kuala Lumpur, Malaysia.
** Corresponding author at: Centre of Polymer Systems, University Institute, Tomas Bata University in Zlín, Trida T. Bati 5678, 760 01, Zlín, Czech Republic.
E-mail addresses: nurazmah.nordin@utm.my (N.A. Nordin), msedlacik@utb.cz (M. Sedlacik).

https://doi.org/10.1016/j.rineng.2025.104753
Received 23 January 2025; Received in revised form 4 March 2025; Accepted 28 March 2025
Available online 29 March 2025

durability, high stiffness and flexibility while keeping the overall weight low [4–6]. Among various types of composite foams available to date, a magnetorheological (MR) foam stands out as a promising candidate for soft gripper devices since they render distinctive magneto-responsive behaviour [7–9]. The ability of the MR foam to reversibly change its viscoelastic behaviour actively and continuously in response to tuneable magnetic fields has piqued interest among researchers to implement semi-active soft gripper devices. Commonly, iron particles or carbonyl iron particles (CIPs) have been utilised as the reinforced particles in the foam matrix. The particles are embedded either directly (in-situ) or indirectly (ex-situ) to consummate the magnetically responsive material [10]. In fact, CIPs have possessed high magnetic saturation, high permeability, low remnant, and a temporary magnetism [11–14] so the properties can be easily controlled. In such a way, the mechanical and rheological properties of the MR foam can be immediately fined-tuned by varying the magnetic field strength. Meanwhile, polyurethane (PU) foam has been widely used as a matrix material for MR foam due to its numerous polymer-composite advantages in terms of storage modulus absorption, flexibility, and mechanical strength. For this reason, PU become as the ideal medium for dynamic applications such as vibration and damping absorption [15–17]. However, the exploration of MR foam on its damping ability are currently limited.

Mechanical vibrations including micro-scale deformations resulting from the dynamic oscillations in the environment, can significantly impact some of the components in soft robotic applications [18,19]. These include the soft robotic grippers and development of the material designed for the particular purpose. In a soft gripper, damping plays a pivotal role in controlling the performance and functionality of the components. Effective damping characteristics are essential to absorb and dissipate the heat energy that is primarily generated during the interaction between the gripper and objects, thereby suppressing the excessive oscillations, and ensuring a stable and precise hold. It is also a way to limit the vibrations which could jeopardize the working principle of the gripper. As the MR foam is a novel material for semi-active soft robotic gripper applications due to its lightweight and high flexibility, it is essential to understand how this material responds to the changes and deformations, particularly in absorbing micro-scale oscillations. Known as damping, this phenomenon is often characterized as energy dissipation by the material [1,18,19]. It is typically expressed as a ratio of loss modulus to the storage modulus and is represented by the loss factor (tanδ) [20,21]. Furthermore, examining the damping behaviour of a MR foam via dynamic mechanical compression and rheological testing under shearing would provide greater information on the viscoelastic behaviour of the material. This includes the energy stored and dissipated under the influence of stress, frequency or magnetic fields induced [22–25]. In addition, these dynamic parameters would provide a valuable insight on the interfacial bonding between various constituents in the MR foam as well as possible phase changes [26] which would affect the resulting damping behaviour of the material.

Several researchers have conducted comparative studies on solid-type MR materials such as MR elastomers (MREs), to examine their damping properties under various parameters including strain, frequency and magnetic fields [27–33]. Unlike MR foam, MRE has a strong and solid structures limiting its flexibility. Aziz et al. [27] have reported a study on the variations of loss factor (tanδ) in silicon-based MREs under the influence of strain and magnetic field sweep, considering different concentrations of CIPs. The study also focused on the unaged and thermally aged samples to investigate the material-temperature dependence of MRE samples. It was reported that the tanδ of the unaged MREs, either with 30 or 60 wt. % of CIPs showed insignificant changes with increasing strains, particularly for lower strains of 1 % indicating that the MREs exhibited predominantly elastic behaviour rather than the viscous one. Thus, with that range of strains (0–1 %), the MREs are capable to store more elastic energy rather than dissipating it. In fact, as the increasing magnetic fields applied to the MREs for lower strains ($<$1 %), the tanδ decreased. This was associated with a higher amount of chain links formation between the CIP–elastomeric matrix interfaces, thus led to stiffer MREs [27]. Other previous studies also stated that the presence of a magnetic field has caused a decrement in the tanδ of MREs attributed to the stronger magnetic forces between the CIPs. Accordingly, this resulting in stiffer MRE behaviour hence lesser energy could be dissipated [30–33]. However, as the strain exceeded 1 %, a rapid increase in the tanδ of both MREs was observed, showing their tendency to dissipate more energy upon greater deformations [27]. Similarly, Chen et al. [28] commented on the damping properties of MRE, reporting that the tanδ could be depended on the distance and friction between the matrix and magnetic particles in the MRE. Although increasing the storage modulus (G') led to stiffer MRE, the damping capability (tanδ), however, should be enhanced when the MRE was subjected to elevated strains as more friction effects were generated within the MRE [28]. On the other hand, Yunus et al. reported that the tanδ of MRE was highly dependent on the exciting frequencies [29]. It was observed that the tanδ of their MRE increased with increasing frequency, indicating that more energy was dissipated at higher frequencies due to the increase in frictions from the interfacial slipping between the CIPs and elastomeric matrix.

Although many studies have investigated the damping behaviour of MR materials, research on the MR foam however remains limited. Notably, a study by Ge et al. [34] which was focused on a PU sponge-reinforced MR material reported decreasing tanδ of the MR foam under the influence of magnetic field. This was due to the higher interaction between the particles and matrix phases during the presence of magnetic field, allowing more elastic energy to be stored rather than dissipated as loss energy [34]. What is more, this PU sponge-reinforced MR material is considered as an ex-situ MR foam where the magnetic particles were not directly embedded into the structure of the PU foam, thus the characteristics of this type of MR foam differ slightly from those of the in-situ MR foam. Due to limitations in MR foam research, comparative findings on the damping behaviour of porous materials can be focused on the composite PU foams with incorporated reinforcing particles. Previous studies reported that the presence of reinforcing particles in a PU foam significantly affected its damping behaviour which was attributed to the alteration of the pore's structure caused by the particles [2,35,36]. The structure of the pores of the foam significantly influences the dynamic mechanical properties with smaller pores storing more elastic energy. Higher degrees of interconnected struts are expected to work as a stiffer structure to maintain the elasticity during the usage of the material which resulted in reduced damping performance. Indeed, Tan et al. [37] found that the tanδ of soybean oil-based PU foam showed a decreasing trend when the size of pores was lowered. This phenomenon has been well agreed with some of the previous studies which reported that higher amounts of energy could be stored in the presence of the particles within the porous materials [2,36,38], signifying the improved elastic behaviour of the composite. Nonetheless, under specific conditions such as increasing the frequency, the tanδ of a PVC foam increased [39], probably due to the increase in friction within the material.

These reported studies, however, provide ambiguous information on whether the stiffer characteristics of a composite foam could result in improved damping behaviour or vice versa. This ambiguity may also apply to the MR foam. Therefore, this research aims to offer a scientific insight into the damping behaviour of MR foams under various input parameters. In order to compromise the enhanced capability to store elastic energy (storage modulus) while investigating its damping performance, this study introduces MR foams that are fabricated under different constraining volumes of foaming process. This research also intends to provide a comprehensive investigation of the dynamic mechanical analysis and rheology of MR foams under the influence of varying frequencies. Simultaneously, it seeks to offer better insights into the potential of MR foam as a base material for soft robotic applications, where the storage modulus and the damping ability can be tuned to the strength of the magnetic fields.

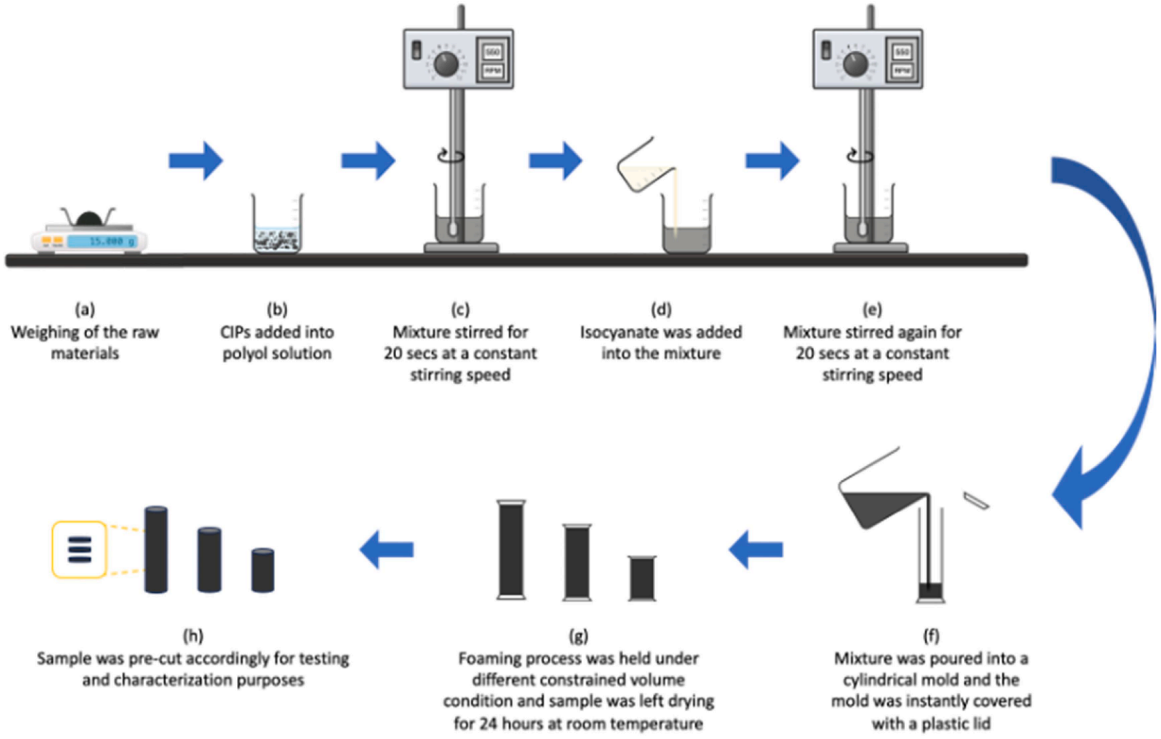

Fig. 1. An illustration of the fabrication process of MR foams.

Table 1
Foaming conditions with the proposed different volume of moulds for fabricating the MR foam samples.

Sample	Foaming condition	Remarks	Density, ρ(g/ml)
PU foam	free foaming	PU foam (without CIPs)	0.20
A	free foaming	MR foam (contain 75 wt. % of CIPs)	0.43
B	100 % volume of constrained foaming	MR foam (contain 75 wt. % of CIPs)	0.45
C	75 % volume of constrained foaming	MR foam (contain 75 wt. % of CIPs)	0.59
D	50 % volume constrained foaming	MR foam (contain 75 wt. % of CIPs)	0.90

2. Experimental method

2.1. Sample preparation

In this study, the in-situ polymerization technique was used to fabricate the MR foam samples. Two essential components are needed to produce the flexible PU foam, specifically, a polyether polyol (PPG)-based triol, as a chemical agent with the density of 1.03 g/ml, and 4,4′-methylene bis(phenyl isocyanate) benzene with the density of 1.00 g/ml acting as a chemical reactant to facilitate the generation of gas bubbles during the foaming process of the MR foam. Both chemicals were provided by Smooth On, Inc. (USA). Meanwhile, OM-grade of CIPs with the average diameter between 3 and 5 μm, purchased from BASF, Ludwigshafen (Germany) was used as the magnetic filler to make the foam magnetically responsive material. The density of the CIPs is approximately 7.87 g/ml. The concentration of the CIPs in the MR foams was kept constant at 75 wt. % as the optimum amount of CIPs in PU foam [7,40,41].

An illustration of the fabrication process of the MR foams for constraint volume foaming process is depicted in Fig. 1. In brief, after weighing the composition of each constituent (a), the CIPs was added into the polyol (b) and the mixture underwent stirring process for 20 s, at a constant speed of 550 rpm (c). Then, the isocyanate was added (d) and the mixture was continuously stirred at the same speed for another 20 s (e). Subsequently, the mixture was poured into the prepared cylindrical moulds of 30 mm diameter with variety volumes of 100 %, 75 % and 50 % (f). The moulds were then immediately covered with PVC lid (g) to induce the constraint foaming condition. The fabricated MR foam samples were left foaming and cured at room temperature of 25 °C, for 24 h. Then, the samples were cut into desired shapes and sizes for further testing and characterizations.

A free-foaming MR foam was prepared as the benchmark for this study as the height of MR foam produced was set as the upper limit for the closed mould height in the constrained foaming process of the MR foams. For the accuracy of the measured height, the fabrication process of MR foam for the free foaming process was repeated a few times to reduce possible human error. The resultant height was then set as 100 % volume of the closed mould for the constraint volume foaming process. Correspondingly, the volume of the closed mould was reduced to 75 % and 50 % from the initial volume, to further investigate the effect of different volumes of constraint foaming process towards the characteristics changes of MR foams. Table 1 displays the information of five fabricated foam samples labelled as PU foam and A, B, C, and D respective to MR foam samples which includes the foaming condition, sample content remarks and their density, ρ. The sample density was calculated using Eq. (1) and the increasing trend of the ρ was observed when different constrained volume foaming processes were applied to the fabrication of the MR foams, as stated in Table 1. As the volume of the closed mould was reduced, the ρ of the MR foams as shown in the table.

$$Density,\ \rho\ (g/ml) = \frac{mass\ of\ sample}{volume\ of\ sample} \quad (1)$$

2.2. Sample testing and characterizations

2.2.1. Dynamic mechanical test of the MR foams

Viscoelastic moduli and loss factor are crucial characteristics of

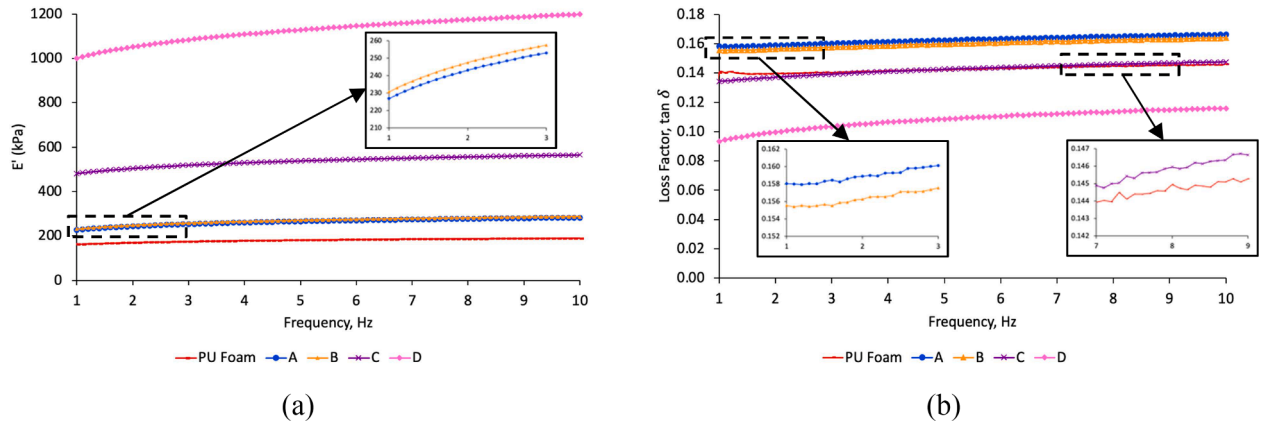

Fig. 2. The frequency dependencies of (a) E' and (b) $tan\delta_{compression}$ towards the MR foam samples via DMA in compression mode.

viscoelastic materials like MR foams, respective to their potential use in soft robotics applications that are frequently subjected to vibrations or kinetic impacts during their operation. In fact, material is considered to have good characteristics when it is capable of both storing energy and efficiently dissipating energy. Therefore, it is crucial to assess the dynamic behaviour and damping characteristics of the MR foams by conducting frequency sweep test to investigate the effect of oscillations towards the resulting modulus of elasticity (E') and loss factor ($\tan\delta_{compression}$) of the materials. Observing how the MR foams respond to the frequency-induced kinetic impacts is important, as even a minor failure would jeopardize their sustainability and potential performance over time [42]. The viscoelastic behaviour of the MR foams in respect to the normal forces was studied by using a dynamic mechanical analyzer (DMA), model DMA1 provided by Mettler Toledo, Greifensee, Switzerland. The tests were conducted under a compression mode, with varying frequencies to observe the damping effect of the fabricated MR foam samples. The carried-out tests adhered to the standard guidelines of the ASTM D5024, specifically a compression test for composite polymers. The DMA was equipped with a circular shaped compression plate a 20 mm diameter. Hence, the fabricated MR foam samples were pre-cut into a cylindrical shaped with the dimension of 2 mm for the thickness and 6 mm for its diameter. A dynamic compression test was conducted with a frequency sweep ranging from 0.1 to 10 Hz while other parameters such as force and displacement amplitudes were set constant at 1 N and 10 μm, respectively. The E' and $\tan\delta_{compression}$ were determined and the data collected during the first 4 min were discarded due to results not being stable as the samples were adapting to a sinusoidal force [26,43,44]. This analysis was conducted to evaluate the impact of different volumes of the constrained foaming process of MR foams towards the mechanical compressive in terms of its damping behaviour. On a side note, all tests were carried out isothermally at room temperature of 25 °C.

2.2.2. Rheological test of the MR foams

Rheological analysis of the MR foams was conducted to analyze the viscoelastic behaviour of MR foams respective to the shear forces, under the oscillatory mode of testing. The tests were carried out by using a Modular Compact Rheometer, model MCR302 from Anton Paar, Austria. To evaluate the effect of dynamic stiffness and the damping behaviour of the fabricated MR foams, the rheological properties of the fabricated MR foams were assessed through frequency sweep tests. The frequency values were varied from 1 to 10 Hz while the other parameters including the strain and operating temperature were kept constant at 0.001 % and 25 °C, respectively. Prior to each test, the samples were cut into a cylindrical shape with the thickness of 1 mm and the diameter of 20 mm. Then, the samples were placed between the parallel plates of the upper rotating disc and bottom stationary base (PP20/MRD/T1). The samples were exposed to two testing conditions which were in the absence of magnetic field (off-state / 0 T) and with the presence of magnetic field (on-state, 0.8 T) to analyze the magnetic response of the MR foam in terms of its storage modulus.

2.2.3. Morphological characterizations of MR foams

A 3D measuring laser microscopy (Olympus, LEXT OLS4100) was utilized to characterize the size of the pores and their distribution in the entire fabricated MR foam samples. This characterization allows a three-dimensional overview of the surface structure of the MR foams which provides information on the measurement of pores and struts structures. Prior to the analysis, the MR foams were cut into a cylindrical shape with thickness and diameter of 1 mm and 20 mm, respectively. Then, the micrograph of each sample was characterized by laser microscopy for a cross-sectional area of the samples. Particularly, images with the scanning area of 2500 μm × 2500 μm were acquired for further analysis. The characterization was carried out at room temperature of 25 °C.

Further, a variable pressure scanning electron microscope (VP-SEM), model JSM-IT300LV from JEOL Ltd, Tokyo (Japan), was utilized to observe a deeper microstructure of the fabricated MR foam samples. In addition to the previous characterization, the VP-SEM has the ability to identify a deeper insight of 2D images of the fine pores, strut structures, and the distribution of magnetic particles which were embedded into the struts of MR foams since it has a high resolution of 3.0 nm at 30 kV, and unsurpassed low kV performance SEM. Prior to the analysis, the MR foam samples with a thickness of 1 mm and 20 mm in diameter were primarily coated with a platinum sputter to prevent any charges effect during the observation. Then, the micrographs were characterized on the cross-sectional area to observe the pores and the strut of the MR foams. Notably, the images were taken under × 100 and × 250 magnifications and all tests were carried out at room temperature of 25 °C.

To complement the microstructural observations by 3D measuring laser microscopy and VP-SEM, a tapping mode of Atomic Force Microscopy (AFM) was used to further investigate the microphase structure (topography) of fabricated MR foams with the sample pre-cut of 6 mm diameter and thickness of 1 mm. The surface topographical evaluations were conducted using a Park FX40, an advance-automated AFM provided by Park System, Suwon (South Korea). This observation was beneficial to evaluate the 3D surface features of the MR foams foamed in the different constraint volumes, within a predetermined scan region of 10 nm × 10 nm, at the scanning rate of 0.14 Hz. The tapping mode analysis was conducted using an aluminium backside-coated cantilever, with a measurement of 10–15 nm tip length and <10 nm radius. Correspondingly, the Park Systems XEI was used to create the microphase images of a localized area, of 20 μm × 20 μm.

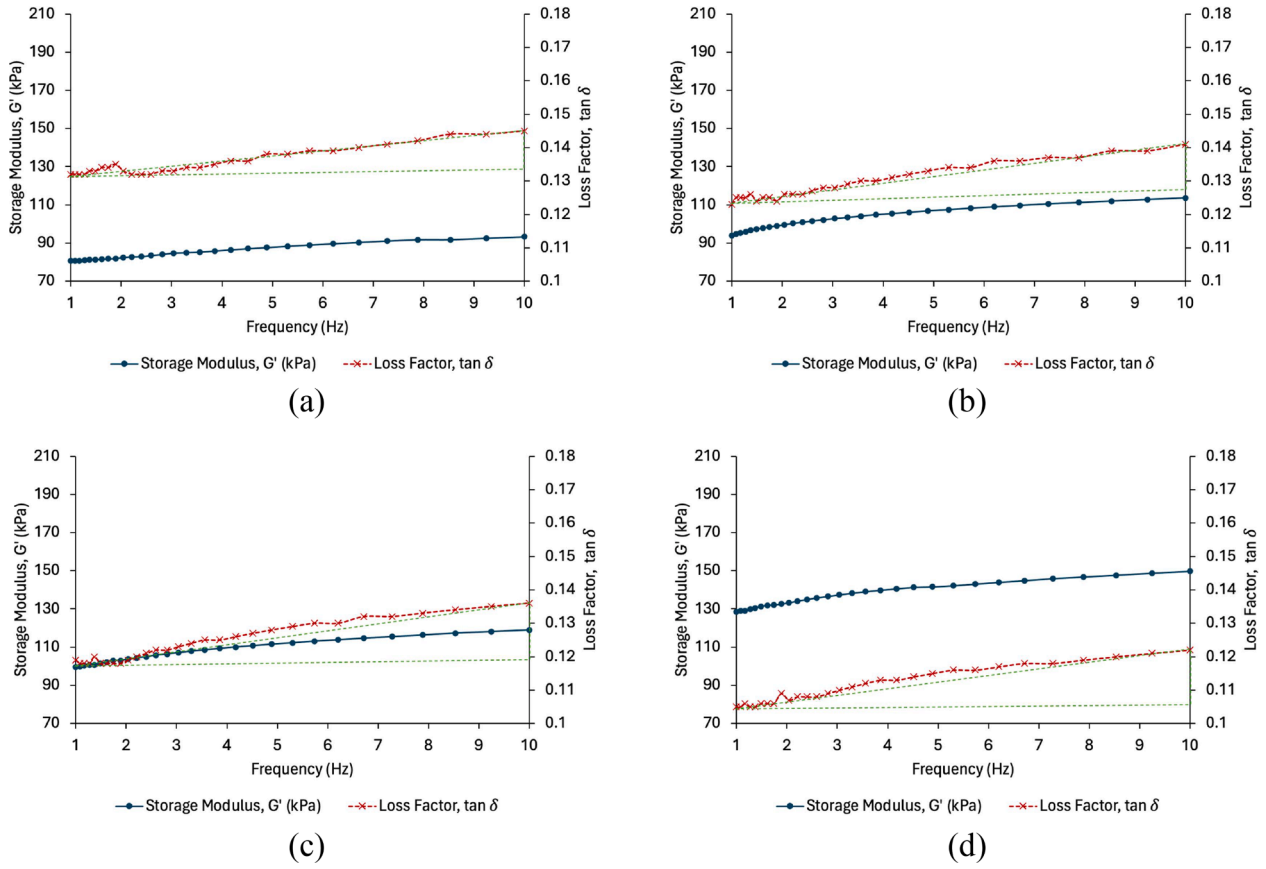

Fig. 3. Frequency dependence of storage modulus and loss factor of MR foams in the off-state (0 A) condition for the fabricated samples: (a) Free foaming process, (b) 100 % of constrained volume foaming process, (c) 75 % of constrained volume foaming process, and (d) 50 % of constrained volume foaming process.

3. Results and discussions

3.1. Dynamic mechanical analysis of MR foams

The dynamic stiffness of the fabricated MR foam samples is measured based on the storage modulus of elasticity (E') which is relative to the frequency increment frequencies, respective to the normal force in compression mode during DMA test.The loss factor ($\tan\delta_{compression}$) of the samples is also projected from the plotted graphs. The frequency dependence of the E' and the corresponding $\tan\delta_{compression}$ at 25 °C are shown in Fig. 2(a) and (b). It can be observed that the MR foams experienced an increase in the $E'$with increasing frequencies. In fact, the pure PU acted as a standard sample exhibited the lowest E' (approximately 158 kPa) compared to the MR foam samples. This observation is expected as fillers generally reinforce the foam structures. The obtained values are also comparable to the previous findings where in general, the E' of the PU foam was in the range of 120 kPa to 210 kPa [45]. Nevertheless, with the presence of CIPs that were embedded into the PU matrix and the foaming process took freely (sample A), the resultant E' was increased by 25 %, i.e. from 158 kPa to 198 kPa. Identically, the E' looked similar when the MR foam underwent 100 % constrained volume during foaming process (sample B), around 199 kPa, as shown in the magnified area of Fig. 2(a) for sample A and B. Then, the E' values were further increased by 125 % (448 kPa) and 300 % (797 kPa) when the volumes of constrained foaming were eventually reduced to 75 % and 50 % from its original volume. The enhancement of E' is attributed to the improvement of CIPs distribution in the fabricated MR foam samples. It is known that when the MR foams undergo foaming process in constrained volumes of a mould, the distribution of CIPs becomes more compact within the constrained volume leading to a formation of a hardened MR foam's structure. The shorter distance between the CIPs caused an increment in the particles-matrix interactions resulting in higher elastic energies stored and distributed in the foam structure hence, higher value of E' could be obtained. The enhancement in E' also indicates the stiffer behaviour of MR foam samples. This finding is in line with the fact that the compression ability of a material increases with the enhanced particle–polymer interactions as well as improved structural characteristic [19].

Despite that, all MR foam samples experienced an increase in $E'$with increasing frequencies. Indeed, sample D shows a distinct increase in E', about 20 % at 10 Hz. The slight increase in the E' with increasing frequency for all samples is anticipated due to the material's response phenomena. At low frequency, the MR foams experienced minor number of oscillations per second allowing the material to respond to the deformations. This caused the sample to exhibit more viscous-like properties, reflected in the lower values of the E'. As the frequency increased, the MR foam experienced more oscillations per second and as a result the samples had less time to respond to the deformations. This did not allow the greater entanglements of the polymer matrix to relax within the samples, leading to an enhanced E' and requiring more energy to be stored [46].

On the other hand, the loss factor ($\tan\delta_{compression}$), which corresponds to the damping behaviour of the samples under a compression mode, shows a similar increment, particularly with increasing frequency as depicted in Fig. 2(b). Generally, the $\tan\delta_{compression}$ increases with increasing frequency [19] and indeed the current samples portray the same trend. As the frequency increased and the MR foams experienced more oscillations per second, the internal structure also underwent greater internal friction, particularly between the CIPs and polymer chains matrix. As a result, more energy is dissipated by the samples in terms of heat. Nevertheless, based on the observation in Fig. 2(b), the higher E' of the MR foam sample led to a lower $\tan\delta_{compression}$. This can be

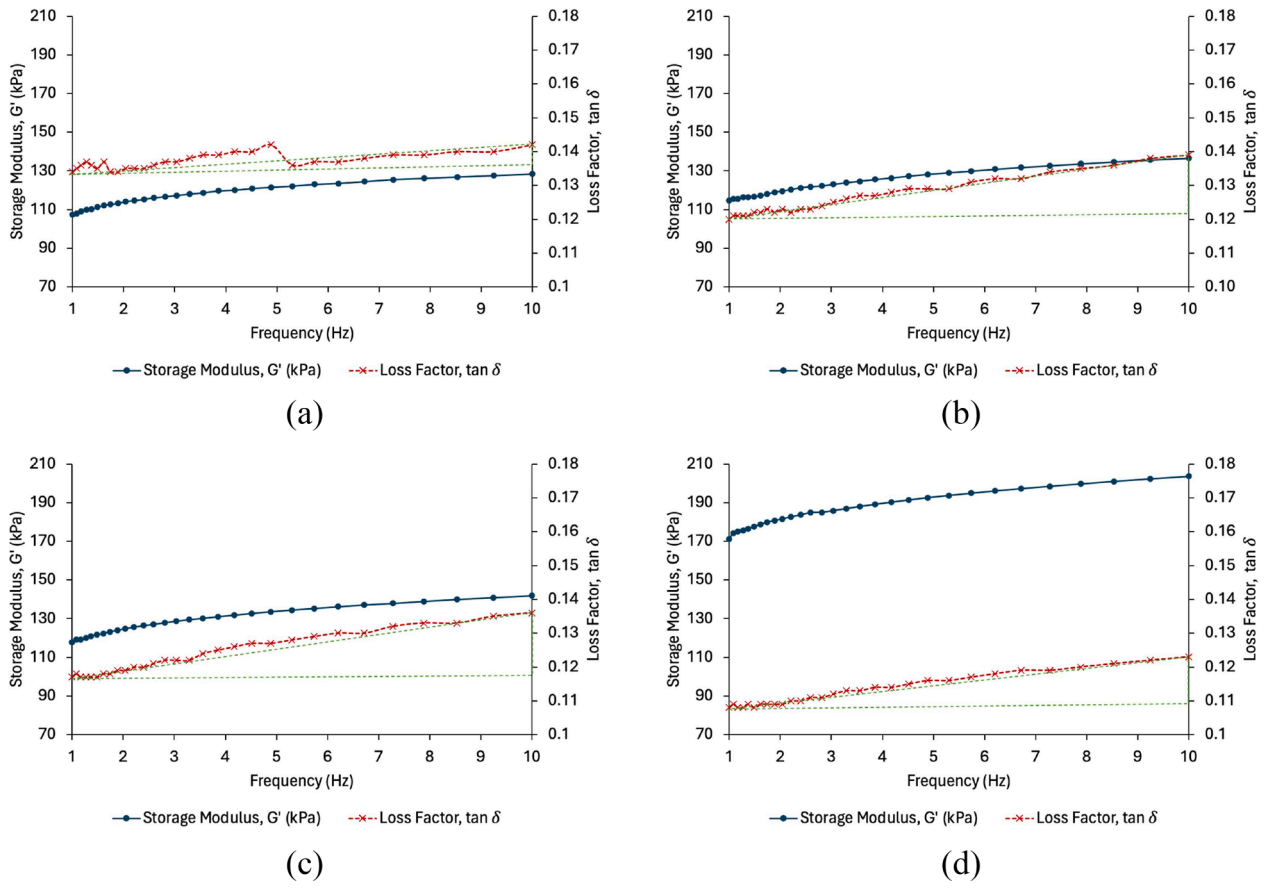

Fig. 4. Frequency dependence of the storage modulus and loss factor of the MR foams during the on-state (4 A) condition for the fabricated samples: (a) free foaming process, (b) 100 % of constrained volume foaming process, (c) 75 % of constrained volume foaming process, and (d) 50 % of constrained volume foaming process.

related to the damping theory where $\tan\delta_{compression}$ will decrease with enhanced stiffness of the samples [47]. The presence of CIPs in the PU matrix allowed the MR foam to gain and store more elastic energy in terms of E'. As the sample behaves more elastically, it compensates to less dissipation energy. Therefore, sample D possess the lowest $\tan\delta_{compression}$, followed by the pure PU foam, samples C, B, and A for the value of 0.094, 0.134, 0.156 and 0.158, respectively. The $\tan\delta_{compression}$ showed a significant increment with frequency indicating that the MR foam has a potential to maintain its improved structural integrity, even after an extended use in applications at higher frequency [47]. Specifically, sample D showed the most pronounced percentage increase of 24 % as compared to sample A which only displayed 5 % of increment within the increasing frequency. The value of $\tan\delta_{compression}$ at 10 Hz were 0.166, 0.164, 0.148 and 0.116 for sample A, B, C and D, respectively.

3.2. Rheological analysis of MR foams

Fig. 3 depicts the storage shear modulus (G') and loss factor ($\tan\delta$) of the fabricated MR foams for (a) sample A, (b) sample B, (c) sample C, and (d) sample D, particularly in the off-state condition. In brief, the G' for all fabricated MR foams increased almost linearly with the increasing frequency, indicating stiffer characteristics of MR foams. It is a typical phenomenon for the G' of the MR foams due to entanglements of polymer chains not being able to relax in the PU matrix [32,33]. The entangled polymer chains do not have the sufficient time to disentangle causing the material to obtain a more elastic behaviour. In addition, the presence of CIPs in the MR foam structure reduced the free spaces among the polymer chains, restricting their motion and thereby enhancing the modulus by providing improved shear strength. In fact, at low frequency of 1 Hz, the initial storage modulus, G'_0 of sample A (Fig. 3(a)) exhibits the lowest value, about 80 kPa. This is due to the response of the material portraying more viscous-like properties rather than elastic-like which indicated lower stiffness characteristics of the MR foam, therefore lower storage modulus. However, at higher frequency of 10 Hz, the storage modulus of sample A increased to approximately 93 kPa. As stated previously, at higher frequencies, the polymer chains have lesser time to move and rearrange, resulting in a more elastic response of the material. Consequently, the material exhibited a higher capacity to store energy, as reflected in the increased storage modulus.

In addition, the G'_0 further increased by approximately 13 % when the constrained volume of foaming process was applied to the MR foam fabrication, as shown by sample B in Fig. 3(b). Besides, as the constrained volume foaming process was further reduced by another 25 % (75 % of initial volume) and 50 % (50 % of initial volume) proportionally to the original volume of the mould (100 %), the G'_0 of the MR foams was enhanced to about 100 kPa and 128 kPa for sample C (Fig. 3 (c)) and sample D (Fig. 3(d)), respectively. The reduced volumes of the constrained foaming process caused a more compact distribution of the CIPs within the structure of MR foams. This resulted in a higher interference of the friction between the particles and matrix, which in turn increased the modulus of the MR foams [48]. The smaller volumes of the mould during the foaming process also caused the number of particles in localized areas to increase, which then affected the formation and growth of the pores in the structure of the MR foams. The changes in structure also resulted in the increment of G' of MR foams which will be further explained in next section. Similarly, at the highest frequency of 10 Hz, the G' of samples B, C, and D were further enhanced to 114 kPa, 119 kPa, and 150 kPa, respectively, showing a greater elastic response of the materials.

On the other hand, the loss factor ($\tan\delta$) of the fabricated MR foams

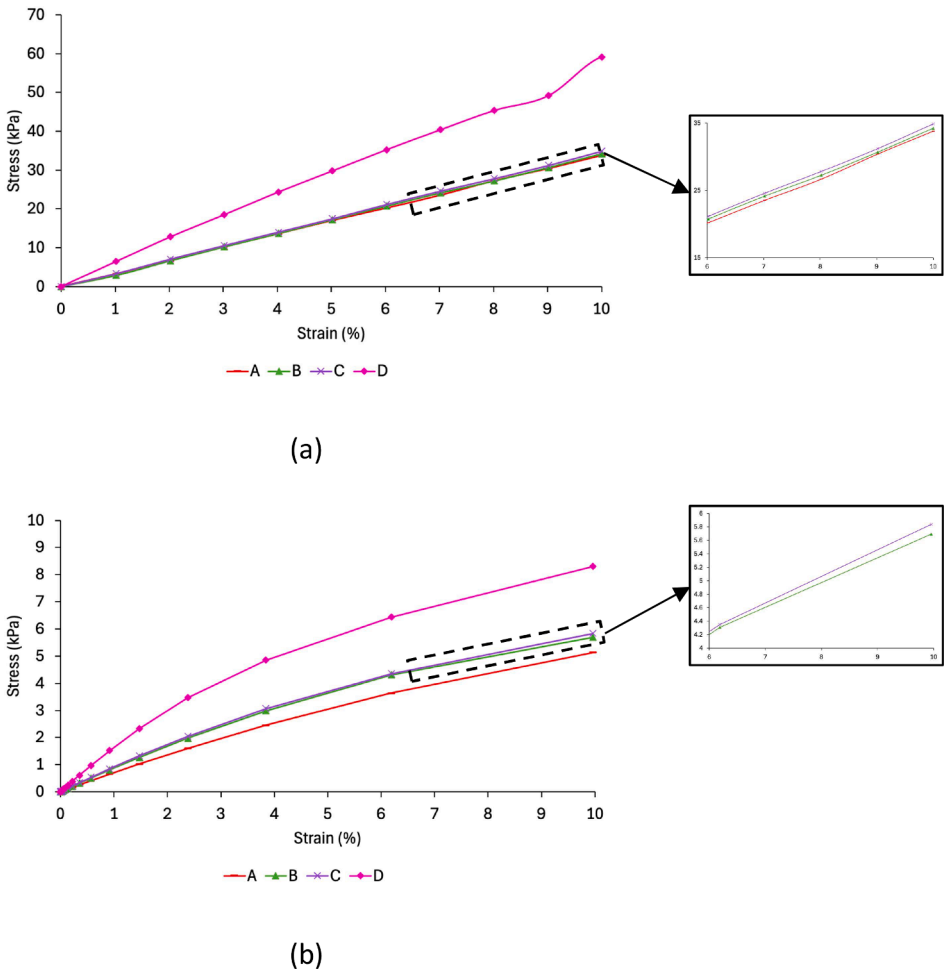

Fig. 5. Stress – strain graphs of the(a) dynamic mechanical-compression and (b) shearing of the MR foams.

samples was gradually increased with increasing frequency. The loss factor (tanδ) is generally defined as the ratio of the loss modulus to the storage modulus of a material and this indicates how effectively the material dissipated energy, where higher tanδ corresponds to a greater damping efficiency. As the frequency increased, the polymer chains of the PU and the embedded CIPs within the MR foam experienced greater rates of deformation. This led to a greater internal friction and energy dissipation through the viscoelastic mechanism, such as the molecular rearrangements and the movement of the polymer chains of the PU foam [32,33,49]. Therefore, the MR foams experienced an increment of their energy dissipation (loss factor) at higher frequencies, as presented in Fig. 3(a) – (d). Nevertheless, the tanδ of the MR foams were observed to decrease respective to the reduction of the constraint volumes foaming during the processing. In fact, at specific frequency of 1 Hz, the tanδ for sample A, B, C, and D are 0.132, 0.123, 0.119, and 0.105, respectively. This is due to the enhancement in the G' of MR foam samples as discussed in previous paragraphs. Reducing the constrained volumes in the foaming process affects the distribution of CIPs, causing the particles to become more compact and reduces the distance between the particles. As a result, the MR foams exhibited a more elastic than viscous behaviour. Thus, slightly more storage energy was recorded instead of being dissipated, i.e. shifting of tanδ to the lower values was noted. The interfacial interactions between the CIPs and the PU foam (particle-matrix interaction) also improved, resulting in a reduced friction between both phases and consequently less energy dissipation [27].

Likewise, when a magnetic field was applied to the MR foam samples, they showed a greater value of G'_0 as depicted in Fig. 4(a) – (d). In general, the results align with our previous findings, showing a similar increasing trend in G' when a magnetic field is applied to the MR materials [33,48,50]. This phenomenon is attributed to the magnetic forces and attraction between the magnetic particles (CIPs) in the MR foam. This interaction should further increase the stress distribution in the material, and correspondingly, the G' increased indicating more energy could be stored elastically [51]. In brief, as the G' of the MR foams increased with the frequency and constrain volumes foaming processes, the effect was more pronounced in the on-state condition due to the additional magnetic attraction between the particles. Furthermore, the increased stress distribution led to a brittle structure and stiffer characteristics of the MR foams, thus enhancing the G'. In addition, in the constraint volumes foaming process of the MR foams, the concentration of the particles at localised area increased, thus reducing the distance between them. Consequently, stronger magnetic forces are present between the particles when a magnetic field (4 A) is applied. Indeed, as shown in Fig. 4(d), the G' of sample D exhibited the highest value, reaching up to 170 kPa at 1 Hz, compared to the other samples in the on-state condition. Meanwhile, reaching up to 10 Hz, the G' of sample A was noted about 128 kPa, followed by 136 kPa, 142 kPa, and 204 kPa for sample B, C and D, respectively.

However, as the MR foams were in the on-state condition and subjected to the reduced constrained volume foaming process, which resulted in stiffer characteristics of the material, the tanδ exhibited a decreasing behaviour in comparison to the off-state, as shown in Fig. 4 (a) – (d). In fact, the tanδ at 1 Hz for sample A was 0.134, followed by sample B, C, and D were 0.120, 0.117, and 0.108, respectively. The lowered values of tanδ for MR foams are attributed to the enhancement of the storage modulus of MR foams that caused the resultant fraction of

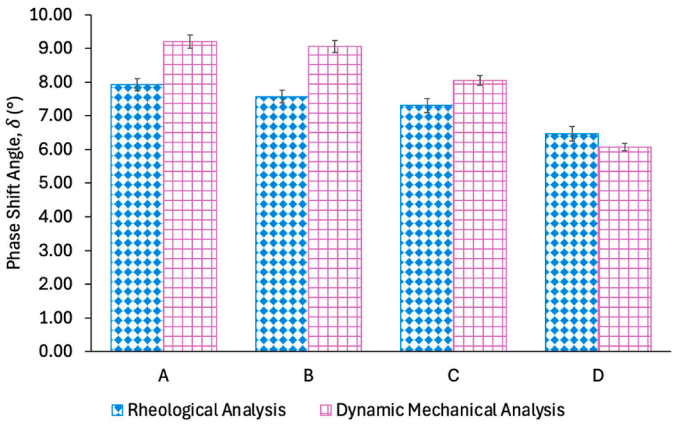

Fig. 6. The phase shift angle (δ) of the MR foams for rheology (shear) and DMA (compression) analyses.

the loss modulus (G'') to the G' reduced. As stated in the previous paragraph, the improvement in the structure of the MR foams with constrained volume foaming during their processing as well as stronger magnetic forces between the CIPs with presence of magnetic field strengthened the interfacial interaction between the CIPs and PU matrix. Thus, the further enhancement of the G'resulted in the MR foams to become more capable of storing more energy rather than dissipating it, as explained from the decline in tanδ [29,32,50,52]. On the other hand, as the applied frequency increased from 1 to 10 Hz, the tanδ of all samples increased indicating a greater rate of deformation occurred in the structure of the MR foam samples. This phenomenon is also similar as in Fig. 3(a) – (d). The dynamic response of the MR foam samples increased, enhancing their energy absorption and dissipation capabilities. This, in turn, contributes to the overall increment of the damping effect of the MR foams. Sample D showed the most ability to dissipate energy upon increasing frequency with the percentage increase of 20 % compared to sample A which only display 9 % of increment. Therefore, based on this analysis, the MR foam has the ability to store more elastic

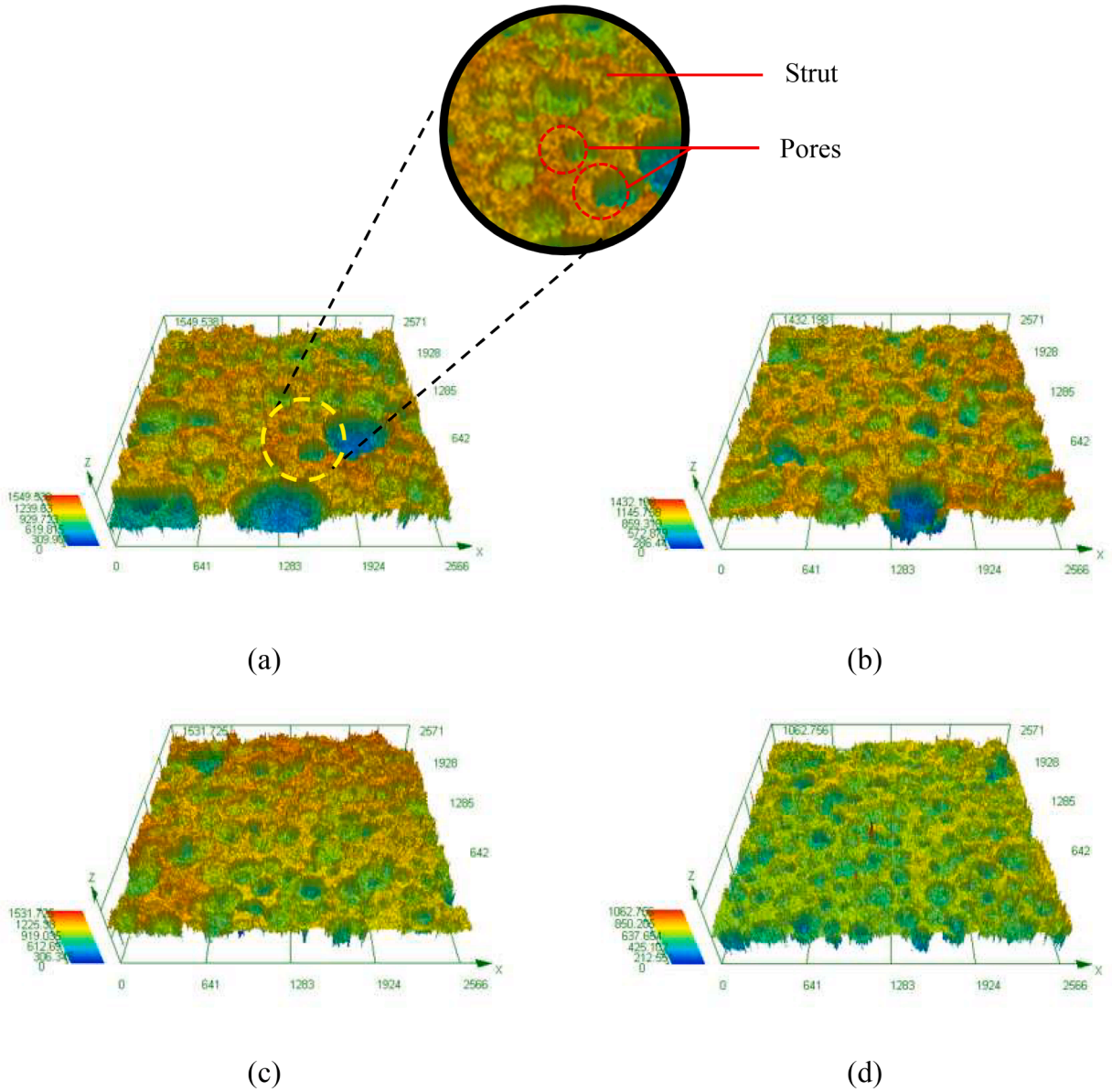

Fig. 7. Surface scanning of the fabricated MR foam samples under the observation of a 3D laser microscope, for sample A (free foaming), B (100 % of constrained volume foaming), C (75 % of constrained volume foaming), and D (50 % of constrained volume foaming). The variation of colours from red (peak) to blue (valley) indicates the mixture of larger and smaller pores with varying depths of the fabricated MR foams.

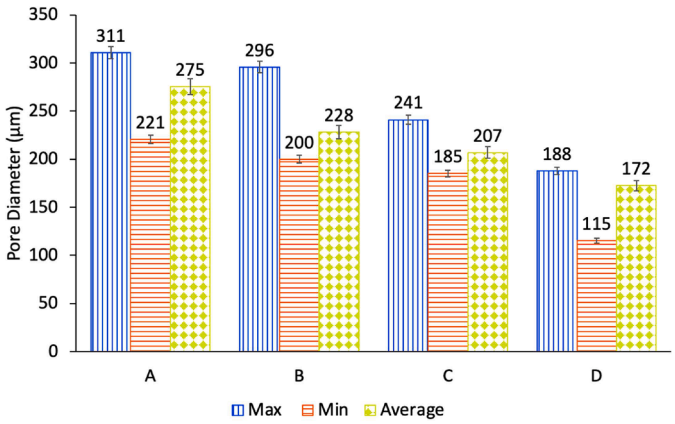

Fig. 8. The bar charts of the maximum, minimum and average diameter of the pores for sample A (free foaming), B (100 % of constrained volume foaming), C (75 % of constrained volume foaming), and D (50 % of constrained volume foaming).

energy (G') as well as possess improve damping characteristics (tanδ), particularly for increasing frequencies which could be the ideal candidate for soft robotic applications to reduce effect of the oscillation during the device operation.

3.3. Correlation between the DMA (Compression) and the rheological (Shear) properties of the MR foams

The DMA and rheology generally measure how materials respond to a deformation under a given stress. When a force is applied to the MR foam, the material deforms respectively to the distributed stress, exhibiting a viscoelastic behaviour with both elastic and viscous characteristics [7,17,41,53,54]. An MR foam would retain the deformation proportionally up to the linear viscoelastic (LVE) limit, beyond which the material deforms in a non-linear way. This means a longer time is required to return to its original state, and the material is also susceptible to fall into a viscous behaviour. For that reason, both the DMA and rheology of the MR foams have been investigated within their LVE region. Although the DMA and rheological test involved different directions of applied force, the resultant properties can be correlated in terms of stress-strain profiles, corresponding to the modulus of elasticity (E' and G') and the loss factor (tanδ), during a frequency sweep test. Fig. 5(a) and (b) depicts the stress – strain graphs for the DMA compression and shearing of the MR foams carried out at 1 Hz. It can be observed that all profiles of all samples showed an increasing trend in stress with increasing strains. In fact, the increasing trends were similar with the previous studies [26,31,55] indicating that stiffer MR foam samples compensate a with greater stress endurance. As stated in the previous sections as well, the stiffer MR foams are attributed to the compact porous structure with the localized CIPs, especially after different constrained volumes of foaming process were applied concurrently that resulted the MR foam's structure to become more compact, firm, and brittle. This, in turn lead to an enhanced E' and G' of the samples. Respective to the Fig. 5(a) or (b) and correlated to the foaming process as stated in Table 1, sample D, which has the most compact porous structure, could withstand the highest elastic stress, followed by sample C, B, and A.

On the other hand, as afore mentioned, the damping behaviour in form of the loss factor (tanδ), can also be interpreted as phase shift angle (δ). The δ typically describes the material's behaviour in terms of elasticity based on the horizontal shift between the sine and cosine graphs, where the sine graph represents the elastic energy stored (E' and G'), while cosine graph refers to the dissipated energy (E'' and G''). Smaller values of δ or lower difference between the sine and cosine graphs mean that the material would dissipate less energy or the material behaves more elastically. In the case of viscoelastic materials like the MR foam, the δ serves as a gauge, where a small value of δ (<45 °) indicates that the material behaves more elastically and solid-like, indirectly suggesting that the material is more capable of storing energy than dissipating it [42]. To complement with the stress-strain profiles as shown in Fig. 5(a) and (b), sample D showed a significantly steeper slope which correlates with the capability of the material to store higher elastic energy with low dissipation. This is also associated with a smaller value of δ, as illustrated in the bar chart of Fig. 6. Similarly, sample D possessed the lowest δ for both the DMA and the rheological analysis. Consequently, the smallest difference between the storage modulus (E' and G') and the loss modulus (G'') were reflected in the sample. As highlighted previously, the higher storage modulus portrayed the stiffer characteristics of the MR foam, therefore sample D had the most compact porous structure with the CIPs distributed within the constrained volume, as compared to the other samples. On the contrary, as shown by sample A, the δ exhibited the highest value indicating most notable difference between E'/G' and dissipated energy. This also corresponded to the behaviour of sample A to store less deformation energy, compared to sample B, C as well as D upon the applied stress.

3.4. Morphological analysis of the MR foams

Fig. 7(a) – (d) present the surface morphology of the fabricated MR foam samples under 3D laser microscopy and information about the average pore diameters are projected in Fig. 8. In brief, the different constrained volumes of foaming process during fabricating the MR foams have impacted their microstructure development. In Fig. 7(a), the porous structure of free foaming MR foam (sample A) displayed distinctly different pore sizes, with an average pore diameter of approximately 275 μm, compared to other MR foam samples. Indeed, the variation of colours from red (peak) to blue (valley) can be observed in sample A which indicates a mix of larger and smaller pores with varying depths, highlighting the imbalanced porous structure of the MR foam. Then, a considerable decline in the average pore diameters were noted for samples B, C, and D, accompanied with an improvement of the homogeneity in terms of a circular shape of the pores. This corresponds to the different constrained volumes of the foaming process. The average pore diameter for sample B was about 228 μm and the average pore value was lowered to 207 μm and 172 μm for sample C and D, as the constrained volumes were further reduced to 50 % and 25 %, respectively. Sample D displayed particularly the most uniform colour throughout the scanned sample, indicating that the pore sizes and their heights were nearly identical. Such effects are attributed to the compared and improved distribution of the CIPs during the constrained foaming which enhanced the heterogeneous nucleating process of the pores. This phenomenon has indirectly produced higher number of the pores with smaller size since the pores could not be expanded within the constrained volume [40,41,53,56,57]. As a result, sample D in Fig. 7(d) possesses the most enhanced surface structure, created by a higher number of smaller pores, which were homogenously distributed in the entire MR foam sample.

In addition, a microscopic analysis by using VP-SEM for all MR foam samples is presented in Fig. 9, firstly (a) showing a typical microstructure for the free foaming sample and secondly the changes of the structure after constrained volumes foaming process, as presented in (b) – (d). Generally, a MR foam consists of the pores enclosed by the struts where the CIPs are located, as labelled in the magnified area of Fig. 9(a). According to the figures as well, all fabricated MR foam samples had open pore structures, which is consistent with the previous study [7]. Sample A in Fig. 9(a) exhibited larger open pore structure compared to the ones fabricated under the constrained volumes foaming process. As the volumes of the constrained foaming decreased from 100 % to 50 %, the size of the pores also decreased, and this observation is corresponding to the tabulated data presented in Fig. 8. In general, the

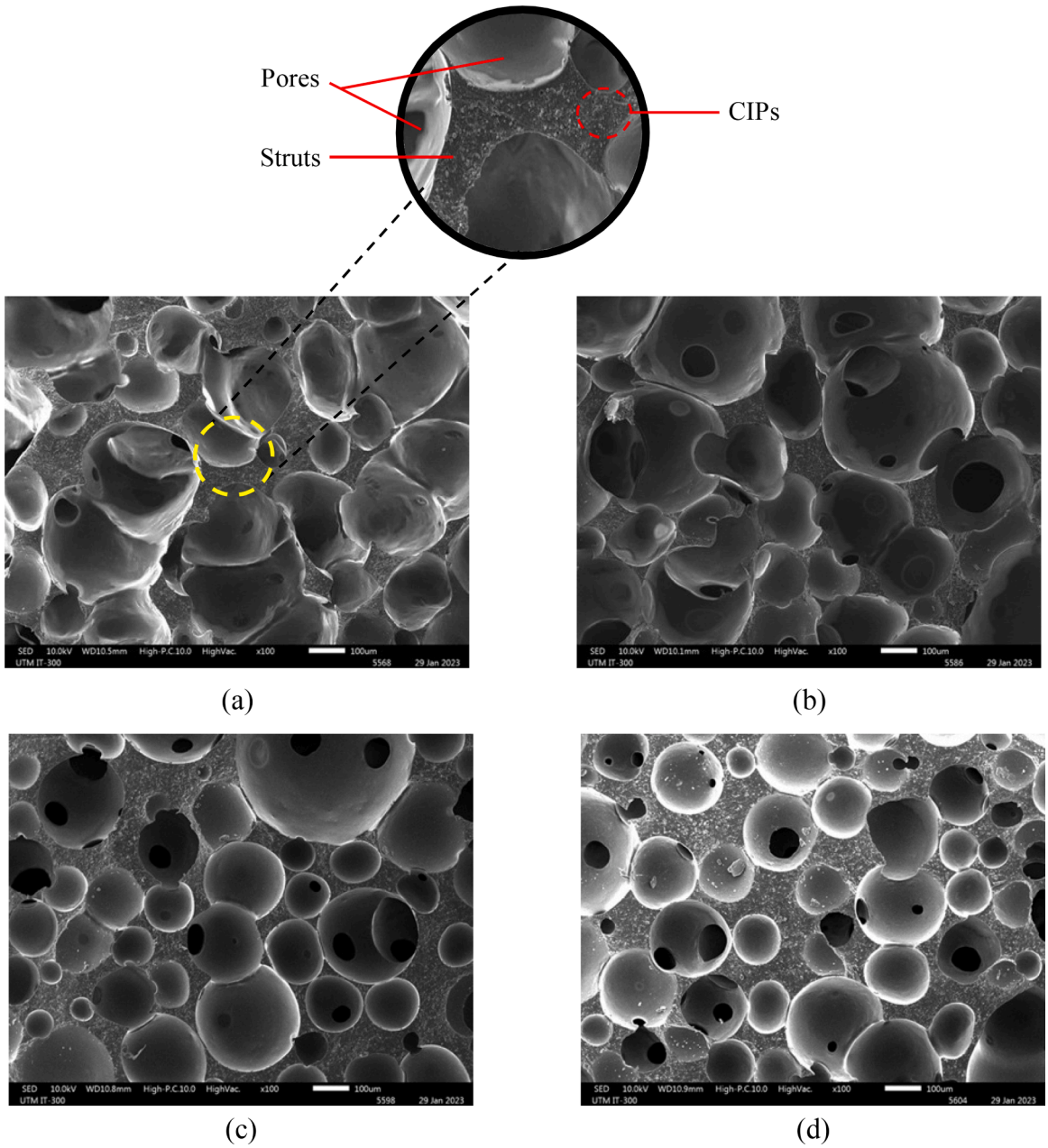

Fig. 9. VP-SEM images showing the pore and strut structures of MR foam samples fabricated via (a) free foaming process and constrained foaming of (b) 100 %, (c) 75 %, and (d) 50 % constrained volumes, respectively.

structure of the foam is mainly influenced by the formation of air pockets (pores) trapped in the foam during foaming process. For the free foaming process of MR foams, the CIPs that were added into the PU liquid acted as a nucleating agent for the formation of the pores. The CIPs concentration facilitated the pores' formation, further manipulating their size and the MR foam growth process [7,56,57]. Respective to Fig. 9(d), which corresponds to sample D, the production of smaller pores was attributed to the higher concentration of the CIPs per unit volume. This led to an improved distribution of CIPs over the composite area which promoted higher formation of pores under the constrained volume condition (50 %). Within the compact area, the growth of pores might be restricted thus, an improved porous structure with smaller pore sizes was observed over the MR foam area. This structure improvement of sample D also led to the enhancement of the storage modulus of the MR foam with a tolerable energy dissipation, providing better dynamic response which aligns with the explanation in the previous sections. Similarly, with the 75 % (sample C) and 100 % (sample B) of constrained volumes foaming process, the localised CIPs became loosen within the area resulting in a reduced formation of pores and larger in sizes during the growth process as shown in Fig. 9(c) and (b), respectively.

To support this finding, an AFM analysis was carried out to further investigate the correlation between the effect of the constrained foaming process towards the distribution of the CIPs in the struts of the fabricated MR foams. The microphase segregation between the phases of the CIPs and the PU matrix was observed and the results were presented in Fig. 10(a) and (b) for sample A and D, respectively. In the phase images obtained by the tapping mode of the AFM, the orange colour (lighter), signifying the rigid domains, representing the CIPs while the greyish-black colour (darker) represents softer domains corresponds to the PU matrix. In brief, the lighter domains that are scattered around the scanning area indicate that the CIPs were well distributed in the struts of both samples. In fact, as discussed in the previous sections, due to a

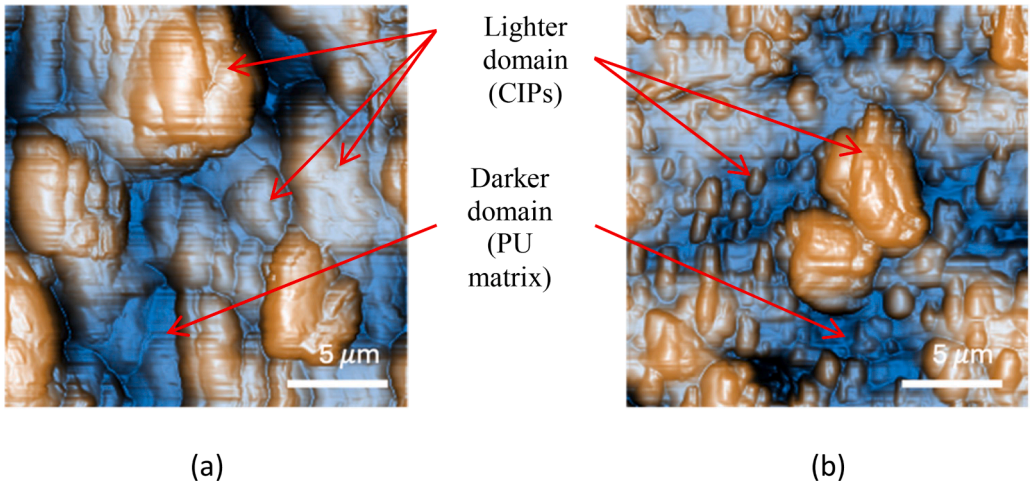

Fig. 10. AFM phase separation images indicating the soft and hard domain of (a) sample A and (b) sample D.

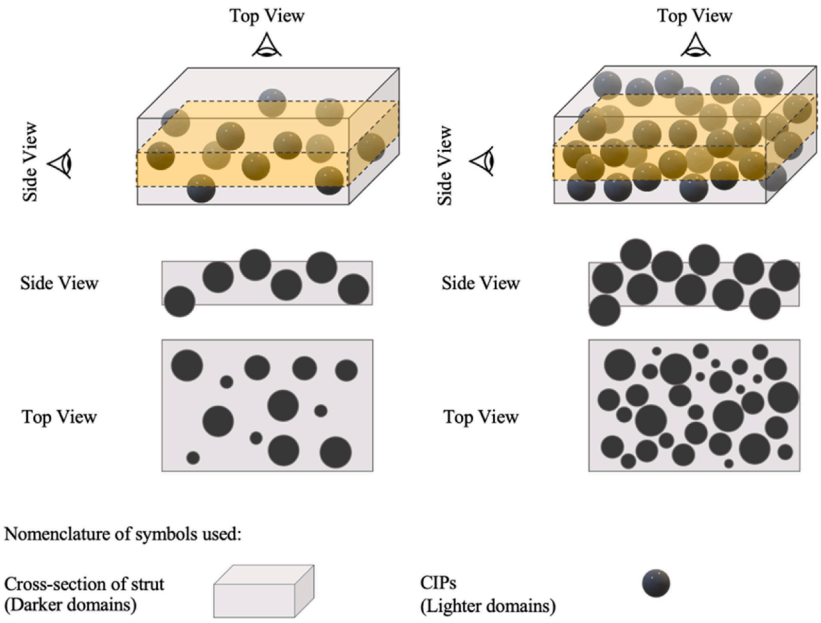

Fig. 11. A schematic illustration of the strut cross-section structure of the MR foam fabricated by (a) free foaming process (sample A) and (b) 50 % of volume of constrained foaming process (sample D).

different foaming process of both samples, the localized CIPs in the struts of sample D are very densely packed as compared to sample A that contained less CIPs due to the free foaming process. Referring to Fig. 10 (a) and (b), the lighter domains (CIPs) of sample A appear to have notably larger distances between the particles compared to sample D which possesses closer distances among the particles and which are observed more frequent. Correspondingly, the concentration of CIPs per unit volume of sample D is higher than sample A which resulted in a higher storage modulus of the MR foam, corresponding to the previous report [53].

Further, the variations in the size of the lighter domains (CIPs) in sample D are attributed to the differences in the depth of the observed struts [58]. Fig. 11(a) and (b) present the schematic diagrams illustrating the distribution of CIPs within the struts of MR foams for samples A and D, respectively, as viewed from different angles. From the top and the side views of sample A, the CIPs are expected to have further distances between the particles, whereas sample D demonstrated compact CIPs is anticipated to show the opposite phenomenon. This is mainly due to the difference in the expansion ratio for both MR foams where the foaming process of sample D has been restricted by 50 % of constrained volume hence the expansion foaming has been limited thus, has more compact distribution of the particles. As more pores with smaller sizes formed, more struts became available to contain the distributed CIPs, which might lead to an increase in the surface area of the struts. As a result, the variations in the depth of the observed struts per unit volume in sample D become more pronounced as compared to sample A. In return, the observation of the lighter domains (CIPs) appeared in a wider range of sizes, as shown in Figs. 10(b) and 11(b).

In terms of the structure changes, the values of modulus (E' and G') of the MR foams are highly dependent on the microstructure after undergoing different constrained volumes of foaming process. As presented in the previous sections, as the E' and the G' were increased, the value of the tanδ was decreased, sequentially for samples A, B, C, and D. As the constrained volumes foaming process was reduced from the free foaming to 100 %, 75 %, and eventually 50 %, smaller pores were observed. As a result, the total surface area of the structures is expected to increase due to the formation of the smaller pores in the MR foams [53]. In fact, the distribution of the CIPs should be denser in the struts of the samples,

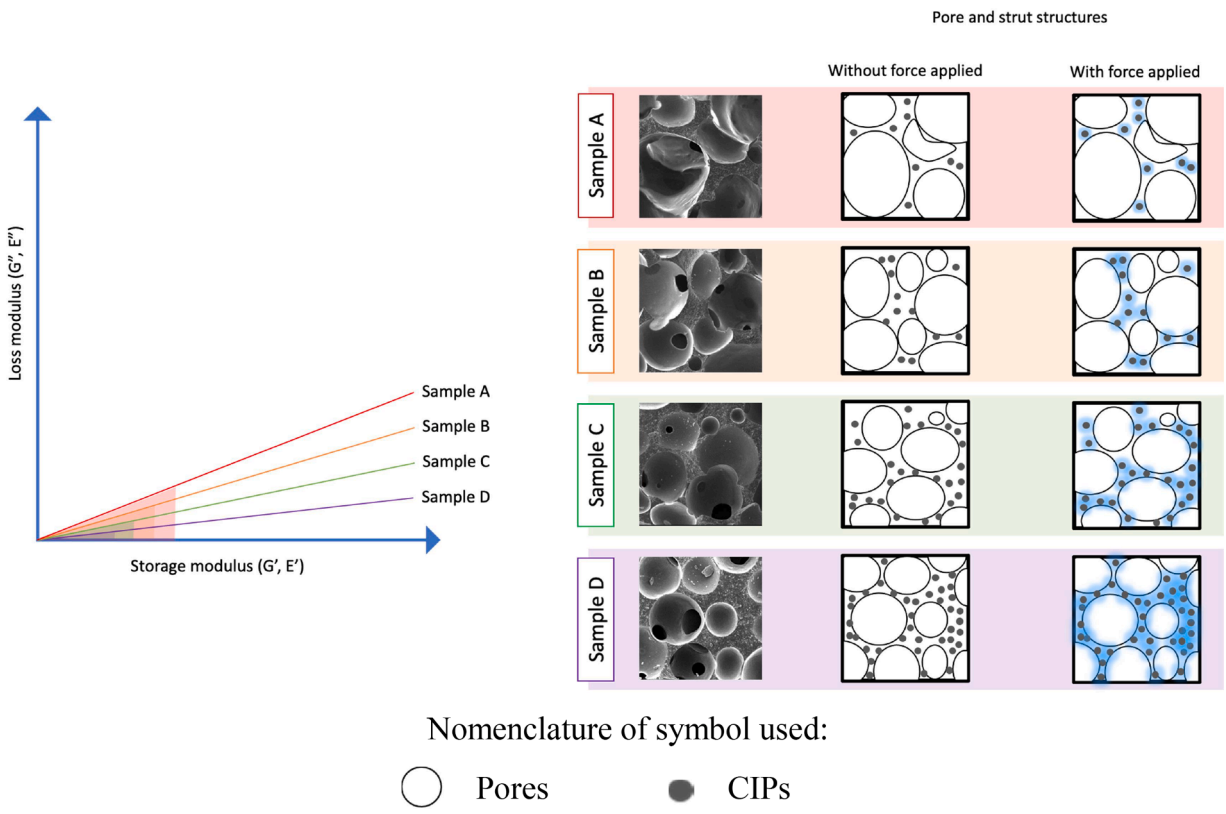

Fig. 12. Illustration mechanism of the correlation between the storage modulus and loss modulus of all MR foams from DMA and rheological characteristics towards its morphological changes.

especially for sample D. Hence, more stress could be stored and distributed within the material as compared to the free foaming sample A. As illustrated in Fig. 12, which is related to the pore and the strut structures in each of the MR foam, the blue shades that outlined the surroundings of the matrix and CIPs indicate the distribution of the elastic energy when the stress was applied to the material. As analyzed above, based on the DMA compression and the shear modulus (E' and G') of each sample, the free foaming sample A displayed the lowest storage modulus with the highest loss modulus (E'' and G''). This is due to the higher amount of gaps between the CIPs and lower surface area of the struts. Thus, the structure shows an improved flexibility as opposed to the constrained volumes foaming process of samples B, C, and D. These three samples, on the other hand, exhibited a gradual increase in the storage modulus, attributed to the more compact porous structure with more localized CIPs, which then enhanced the stiffness of the materials. The structure of sample D also became firmer thus had more capability to store elastic energy distributed throughout the rigid structure and was improved in resisting a deformation. In return, the capability of the dissipating energy was reduced, as shown in Fig. 12. Nevertheless, in the discussion of Figs. 2 and 3, with increasing frequency, the MR foams foamed under the constrained foaming process, particularly sample D, possessed an improved loss modulus or loss factor (tanδ) due to greater friction phenomenon within the compact structure of the MR foam. Consequently, this leads to a more pronounced increase in the tanδ upon increasing frequency, when compared to sample A.

4. Conclusion

In this study, MR foams with 75 wt. % content of CIPs were prepared via an in-situ polymerization method under two conditions: the free foaming and the different volumes of constrained foaming process. Following, the samples were labelled as A, B, C, and D for the MR foams fabricated through the free foaming and the constrained foaming of 100 %, 75 %, and 50 % of volume, respectively. The analysis of the dynamic mechanical compression and the shear rheology under varying frequencies showed that the MR foams prepared under the constrained volumes foaming process, in particular at 50 %, exhibited significant enhancements in the elastic moduli (E' and G') and the loss factor (tanδ) of the material. Under a dynamic mechanical compression analysis, the presence of constrained foaming during the fabrication process of the MR foams contributed to an approximately 25 % increment on the initial E' as compared to the free foaming sample. In fact, with the further volume reduction of 25 % and 50 %, it further increased by about 125 % and 300 %. A similar trend could be observed for the rheological analysis, where 13 % increment of G' can be seen when the constrained foaming was introduced. Overall, it was observed that under the influence of increasing frequency, the storage modulus for all MR foam samples showed a rising trend for both the dynamic mechanical compression and the shear rheology. The reduced volumes of constrained foaming process caused that a higher interference friction between the particles and matrix was produced. This resulted in increasing the modulus of the MR foams. It is interesting to note that the tanδ of MR foams also portrayed an increment upon a higher frequency due to the polymer chains of PU and the embedded CIPs inside the foam, the structure experienced a greater rate of deformation. In contrast, the tanδ decreased when the constrained foaming was introduced, additionally the values further reduced with the decreasing volume. This reflected to the higher value of storage modulus shown by the MR foam hence, an enhanced ability to store elastic energy rather than dissipating it. Lastly, the application of a magnetic field during the rheological analysis amplified these effects by showing an increase in the storage modulus and reducing the tanδ, thereby enhancing the mechanical properties of the MR foams. These findings underscore the potential of the MR foams in advanced applications requiring high energy storage and damping capabilities, making them suitable for innovative solutions in various technological fields such as soft robotics applications.

CRediT authorship contribution statement

Ainaa Amirah Marzuki: Writing – review & editing, Writing – original draft, Methodology, Investigation, Formal analysis. **Nur Azmah Nordin:** Writing – review & editing, Supervision, Project administration, Investigation, Funding acquisition, Formal analysis, Data curation. **Saiful Amri Mazlan:** Validation, Supervision, Resources, Project administration, Conceptualization. **Mohd Aidy Faizal Johari:** Writing – review & editing, Validation, Methodology, Investigation, Data curation. **Michal Sedlacik:** Visualization, Resources, Funding acquisition, Conceptualization. **Siti Aishah Abdul Aziz:** Validation, Methodology, Data curation, Conceptualization. **Abdul Yasser Abd Fatah:** Visualization, Software, Resources. **Shahir Mohd Yusuf:** Visualization, Software, Resources.

Declaration of competing interest

The authors declare that they have no known competing financial interests or personal relationships that could have appeared to influence the work reported in this paper.

Acknowledgements

This work was supported by Higher Institution Centre of Excellence (HiCOE) program of Ministry of Higher Education (MOHE) Malaysia under HiCOE Research Grant. The authors would like to acknowledge the financial support from the UTM Fundamental Research Grant (Vot. No. 23H17). Author M.S. wishes to thank the Czech Science Foundation [23-07244S] for the financial support. The authors also would like to thank Mr. Andrei Munteanu for his advice during the writing process.

Data availability

Data will be made available on request.

References

[1] S. Zaidi, M. Maselli, C. Laschi, M. Cianchetti, Actuation technologies for soft robot grippers and manipulators: a review, Curr. Robot. Reports. 2 (2021) 355–369.
[2] V. Dolomanova, J.C.M. Rauhe, L.R. Jensen, R. Pyrz, A.B. Timmons, Mechanical properties and morphology of nano-reinforced rigid PU foam, J. Cell. Plast. 47 (2011) 81–93.
[3] A.K.A. Khalil, Y.H. Teow, M.S. Takriff, A.L. Ahmad, M.A. Atieh, Recent developments in stimuli-responsive polymer for emerging applications: a review, Results Eng 25 (2025) 103900.
[4] W. Li, X. Yang, C. He, J. Sha, C. Shi, J. Li, N. Zhao, Compressive responses and strengthening mechanisms of aluminum composite foams reinforced with graphene nanosheets, Carbon NY 153 (2019) 396–406.
[5] G. Sung, J.H. Kim, Influence of filler surface characteristics on morphological, physical, acoustic properties of polyurethane composite foams filled with inorganic fillers, Compos. Sci. Technol. 146 (2017) 147–154.
[6] G. Sung, J.W. Kim, J.H. Kim, Fabrication of polyurethane composite foams with magnesium hydroxide filler for improved sound absorption, J. Ind. Eng. Chem. 44 (2016) 99–104.
[7] R.E. Mohamed Khaidir, N.A. Nordin, S.A. Mazlan, H. Abd Rahman, S.A. Abdul Aziz, Ubaidillah, N. Nazmi, Stiffness enhancement of magnetorheological foam by structural modification using silica nanoparticles additive, Front. Mater. 9 (2022) 1–14.
[8] L.O.-S. Co Ting Keh, J. Zang, X. Zhao, Magneto-rheological foams capable of tunable energy absorption, in: 2013 Proc. IEEE Southeastcon, IEEE, 2013, pp. 1–3.
[9] S. Kim, P. Kim, S.-H. Choi, J.-S. Oh, S.-B. Choi, Tactile device utilizing a single magnetorheological sponge: experimental investigation, in: W.-H. Liao (Ed.), Act. Passiv. Smart Struct. Integr. Syst. 2015, 2015 94311.
[10] Y. Fu, Z. Wan, G. Zhao, W. Jia, H. Zhao, Flexible conductive sodium alginate/chitosan foam with good mechanical properties and magnetic sensitivity, Smart Mater. Struct. 30 (2021) 075027.
[11] B.J. Park, F.F. Fang, H.J. Choi, Magnetorheology: materials and application, Soft. Matter. 6 (2010) 5246.
[12] J.R. Morillas, J. de Vicente, Magnetorheology: a review, Soft. Matter. 16 (2020) 9614–9642.
[13] T. Huu Nam, I. Petríková, B. Marvalová, Effects of loading rate, applied shear strain, and magnetic field on stress relaxation behavior of anisotropic magnetorheological elastomer, Mech. Adv. Mater. Struct. 29 (2022) 2984–2998.
[14] M.A.F. Johari, I. Aznam, S.A. Mazlan, U. Ubaidillah, N.A. Nordin, S.M. Yusuf, N. H. Lazim, S.A.A. Aziz, Unveiling the Influence of natural weathering on the nanomechanical properties of magnetorheological elastomers, Results Eng. 24 (2024) 103610.
[15] N. Boumdouha, Z. Safidine, A. Boudiaf, A new study of dynamic mechanical analysis and the microstructure of polyurethanefoams filled, Turkish J. Chem. 46 (2022) 814–834.
[16] S.H. Baek, J.H. Kim, Polyurethane composite foams including silicone-acrylic particles for enhanced sound absorption via increased damping and frictions of sound waves, Compos. Sci. Technol. 198 (2020) 108325.
[17] Q. Gong, J. Wu, X. Gong, Y. Fan, H. Xia, Smart polyurethane foam with magnetic field controlled modulus and anisotropic compression property, RSC Adv. 3 (2013) 3241–3248.
[18] M. Pöschl, M. Vašina, Study of the mechanical, sound absorption and thermal properties of cellular rubber composites filled with a silica nanofiller, Materials (Basel) 14 (2021) 7450.
[19] M. Pöschl, M. Vašina, P. Zádrapa, D. Měřínská, M. Žaludek, Study of carbon black types in SBR rubber: mechanical and vibration damping properties, Materials (Basel) 13 (2020) 2394.
[20] M.C. Saha, M.E. Kabir, S. Jeelani, Enhancement in thermal and mechanical properties of polyurethane foam infused with nanoparticles, Mater. Sci. Eng. A. 479 (2008) 213–222.
[21] D.J.T. Hill, M.C.S. Perera, P.J. Pomery, H.K. Toh, Dynamic mechanical properties of networks prepared from siloxane modified divinyl benzene pre-polymers, Polymer (Guildf) 41 (2000) 9131–9137.
[22] X. Liu, D. Zhu, J. Lin, Y. Zhang, Temperature and frequency dependence of the dynamic viscoelastic properties of silicone rubber, Polymers (Basel) 15 (2023) 3005.
[23] S.Sand Chee, M. Jawaid, The effect of bi-functionalized MMT on morphology, thermal stability, dynamic mechanical, and tensile properties of epoxy/organoclay nanocomposites, Polymers (Basel) 11 (2019) 2012.
[24] P. Sathyaseelan, P. Sellamuthu, L. Palanimuthu, Dynamic mechanical analysis of areca/kenaf fiber reinforced epoxy hybrid composites fabricated in different stacking sequences, Mater, Today Proc. 39 (2021) 1202–1205.
[25] J.L. Rivera-Armenta, T. Heinze, A.M. Mendoza-Martínez, New polyurethane foams modified with cellulose derivatives, Eur. Polym. J. 40 (2004) 2803–2812.
[26] S.S. Chee, M. Jawaid, O.Y. Alothman, H. Fouad, Effects of nanoclay on mechanical and dynamic mechanical properties of bamboo/kenaf reinforced epoxy hybrid composites, Polymers (Basel) 13 (2021) 395.
[27] S.A.A. Aziz, S.A. Mazlan, U. Ubaidillah, N. Mohamad, M. Sedlacik, N.A. Nordin, N. Nazmi, Loss factor behavior of thermally aged magnetorheological elastomers, Materials (Basel) 14 (2021) 4874–4889.
[28] L. Chen, X. Gong, W. Li, Damping of Magnetorheological Elastomers, Chinese J. Chem. Phys. 21 (2008) 581–585.
[29] N.A. Yunus, S.A. Mazlan, S.B. Choi, Ubaidillah, F. Imaduddin, S.A. Abdul Aziz, M. H. Ahmad Khairi, Rheological properties of isotropic magnetorheological elastomers featuring an epoxidized natural rubber, Smart Mater. Struct. 25 (2016) 107001.
[30] M. Kallio, T. Lindroos, S. Aalto, E. Järvinen, T. Kärnä, T. Meinander, Dynamic compression testing of a tunable spring element consisting of a magnetorheological elastomer, Smart Mater. Struct. 16 (2007) 506–514.
[31] Y. Fan, X. Gong, S. Xuan, W. Zhang, J. Zheng, W. Jiang, Interfacial friction damping properties in magnetorheological elastomers, Smart Mater. Struct. 20 (2011) 035007.
[32] N. Hapipi, S.A. Mazlan, S.A.A. Aziz, U. Ubaidillah, S.-B. Choi, Effect of curing current on stiffness and damping properties of magnetorheological elastomers, Int. J. Sustain. Transp. Technol. 1 (2018) 51–58.
[33] A.A. Zainudin, N.A. Yunus, S.A. Mazlan, M.K. Shabdin, S.A. Abdul Aziz, N. A. Nordin, N. Nazmi, M.A. Abdul Rahman, Rheological and resistance properties of magnetorheological elastomer with cobalt for sensor application, Appl. Sci. 10 (2020) 1638.
[34] L. Ge, S. Xuan, G. Liao, T. Yin, X. Gong, Stretchable polyurethane sponge reinforced magnetorheological material with enhanced mechanical properties, Smart Mater. Struct. 24 (2015) 037001.
[35] M. Antunes, V. Realinho, J.I. Velasco, Foaming behaviour, structure, and properties of polypropylene nanocomposites foams, J. Nanomater. 2010 (2010) 1–11.
[36] A.R. Hamilton, O.T. Thomsen, L.A.O. Madaleno, L.R. Jensen, J.C.M. Rauhe, R. Pyrz, Evaluation of the anisotropic mechanical properties of reinforced polyurethane foams, Compos. Sci. Technol. 87 (2013) 210–217.
[37] S. Tan, T. Abraham, D. Ference, C.W. Macosko, Rigid polyurethane foams from a soybean oil-based Polyol, Polymer (Guildf) 52 (2011) 2840–2846.
[38] L. Jin, H. Wang, Y. Yang, Polyurethane composites in situ molecularly reinforced by supramolecular nanofibrillar aggregates of sorbitol derivatives, Compos. Sci. Technol. 79 (2013) 58–63.
[39] K. Kanny, H. Mahfuz, L.A. Carlsson, T. Thomas, S. Jeelani, Dynamic mechanical analyses and flexural fatigue of PVC foams, Compos. Struct. 58 (2002) 175–183.
[40] N.S. Muhazeli, N.A. Nordin, U. Ubaidillah, S.A. Mazlan, S.A. Abdul Aziz, N. Nazmi, I. Yahya, Magnetic and tunable sound absorption properties of an in-situ prepared magnetorheological foam, Materials (Basel) 13 (2020) 5637–5652.
[41] R. Norhaniza, S.A. Mazlan, U. Ubaidillah, M. Sedlacik, S.A.A. Aziz, N. Nazmi, K. Homma, S. Rambat, Sensitivities of rheological properties of magnetoactive foam for soft sensor technology, Sensors 21 (2021) 1660–1678.
[42] M.A.F. Johari, S.A. Mazlan, N.A. Nordin, S.-B. Choi, S.A.A. Aziz, S. Daud, I. Bahiuddin, Morphological effects of strain localization in the elastic region of magnetorheological elastomers, Materials (Basel) 15 (2022) 8565.

[43] M. Jawaid, S.S. Chee, M. Asim, N. Saba, S. Kalia, Sustainable kenaf/bamboo fibers/clay hybrid nanocomposites: properties, environmental aspects and applications, J. Clean. Prod. 330 (2022) 129938.
[44] S.S. Chee, M. Jawaid, M.T.H. Sultan, O.Y. Alothman, L.C. Abdullah, Thermomechanical and dynamic mechanical properties of bamboo/woven kenaf mat reinforced epoxy hybrid composites, Compos. Part B Eng. 163 (2019) 165–174.
[45] N.A. Muhayudin, K.S. Basaruddin, F. McEvoy, A. Tansey, Evaluating compressive properties and morphology of expandable polyurethane foam for use in a synthetic paediatric spine, J. Mater. Res. Technol. 9 (2020) 2590–2597.
[46] M. Bek, J. Gonzalez-Gutierrez, C. Kukla, K. Pušnik Črešnar, B. Maroh, L. Slemenik Perše, Rheological behaviour of highly filled materials for injection moulding and additive manufacturing: effect of particle material and loading, Appl. Sci. 10 (2020) 7993.
[47] M. Vašina, M. Pöschl, P. Zádrapa, A study of significant factors affecting viscoelastic damping properties of polymer materials, Manuf. Technol. 18 (2018) 523–529.
[48] N. Mohamad, S.A. Mazlan, Ubaidillah, S.B. Choi, S.A. Abdul Aziz, M. Sugimoto, The effect of particle shapes on the field-dependent rheological properties of magnetorheological greases, Int. J. Mol. Sci. 20 (2019) 1525.
[49] N. Hapipi, S.A. Abdul Aziz, S.A. Mazlan, S.B. Choi, Ubaidillah, N. Mohamad, M. H. Ahmad Khairi, A.Y. Abd Fatah, The field-dependent rheological properties of plate-like carbonyl iron particle-based magnetorheological elastomers, Results Phys. 12 (2019) 2146–2154.
[50] N.M. Hapipi, S.A. Mazlan, M.H.A. Khairi, N. Mohamad, The damping properties of plate-like magnetorheological elastomer, Key Eng. Mater. 772 (2018) 56–60.
[51] R.Z.A. Rashid, N.A. Yunus, S.A. Mazlan, N. Johari, S.A.A. Aziz, N.A. Nordin, M.H. A. Khairi, M.A.F. Johari, Temperature dependent on mechanical and rheological properties of EPDM-based magnetorheological elastomers using silica nanoparticles, Materials (Basel) 15 (2022) 2556–2571.
[52] A.V. Chertovich, G.V. Stepanov, E.Y. Kramarenko, A.R. Khokhlov, New Composite Elastomers with Giant Magnetic Response, Macromol. Mater. Eng. 295 (2010) 336–341.
[53] A.A. Marzuki, N.A. Nordin, S.A. Mazlan, M.A.F. Johari, R.E. Mohamed Khaidir, M. Sedlacik, Ubaidillah, Enhancement of the rheological properties of magnetorheological foam via different constraint volumes foaming approach, Polym. Test. 128 (2023) 108235.
[54] V. Volpe, M. D'Auria, L. Sorrentino, D. Davino, R. Pantani, Injection molding of magneto-sensitive polymer composites, Mater. Today Commun. 15 (2018) 280–287.
[55] R. Guan, H. Zheng, Q. Liu, K. Ou, D. Li, J. Fan, Q. Fu, Y. Sun, DIW 3D printing of hybrid magnetorheological materials for application in soft robotic grippers, Compos. Sci. Technol. 223 (2022) 109409.
[56] R. Norhaniza, S.A. Mazlan, S.A. Abdul Aziz, N.A. Nordin, Ubaidillah, N. S. Muhazeli, Relationship between the response of microscopic and magnetic properties with highly uniform dispersion of carbonyl iron particles in magnetorheological polyurethane foam, Smart Mater. Struct. 29 (2020) 115012–115021.
[57] N.S. Muhazeli, N.A. Nordin, S.A. Mazlan, N. Rizuan, S.A. Abdul Aziz, A.Y. Abd Fatah, Z. Ibrahim, U. Ubaidillah, S.-B. Choi, Characterization of morphological and rheological properties of rigid magnetorheological foams via in situ fabrication method, J. Mater. Sci. 54 (2019) 13821–13833.
[58] M.A.F. Johari, S.A. Mazlan, S.A. Abdul Aziz, N. Zaini, N.A. Nordin, U. Ubaidillah, R.V. Upadhyay, S.Mohd Yusuf, Morphological features of magnetorheological elastomer degradation under a natural weathering environment, Sci. Rep. 14 (2024) 1155.